Advances in Science and Technology Research Journal

Advances in Science and Technology Research Journal, 2026, 20(3), 181–196
https://doi.org/10.12913/22998624/213959
ISSN 2299-8624, License CC-BY 4.0

Received: 2025.09.20
Accepted: 2025.12.04
Published: 2026.02.01

Investigation effect of copper particle size and jaw geometric configurations on jaw crusher wear

Leandro Coloma[1], Rodrigo Sucasaca[1], Jorge Luis Apaza[1], Yuri Silva Vidal Lester[1], Angel Joel Mendoza Quispe[1], Christofer Alex Diaz Arapa[1*]

[1] Department of Mechanical Engineering, Universidad Nacional de San Agustín de Arequipa, Santa Catalina 117, Arequipa 04000, Peru
* Corresponding author's e-mail: cdiazar@unsa.edu.pe

ABSTRACT

The growing demand for efficiency in industrial crushing processes has highlighted the need to understand the particle behaviour in jaw crushers in order to minimise wear and maximise productivity. In response, analysing the influence of particle size and jaw geometry can play a crucial role in reducing operating costs and increasing equipment life. This study explored the relationship between different material sizes as well as the geometric configurations of movable and fixed jaws in the wear of jaw crushers. A comparative analysis was performed using simulation to evaluate wear through a discrete element method-multibody dynamics-particle replacement method (DEM-MBD-PRM) coupling with the Tavares fracture model and the Archard wear model. Prior to simulation, the material and contact parameters were calibrated in EDEM software to ensure reliable representation of copper–steel interactions. This analysis process led to a better understanding of tribological behaviour. The configurations with smaller particle sizes, in the range of 80 to 100 mm, reduced wear by up to 50% compared with larger particles, in the range of 100 to 120 mm, with distinct wear patterns observed between sharp and standard profiles. Additionally, simulation showed that jaws with sharp profiles typically had longer service lives, suggesting that the configurations with standard profiles and large particle sizes are the most susceptible to wear. The findings of this study demonstrate that optimising feed particle size and jaw geometry can reduce wear on crusher components by up to 50%, directly contributing to more efficient crushing operations, extended equipment lifetime, and lower maintenance costs. Although the study was uniquely based on computational modelling without an experimental verification, the results provide a solid framework for the guidance of future physical testing and design improvements.

Keywords: jaw crusher, discrete element method, copper particle size, jaw crusher wear, jaw geometric configuration.

INTRODUCTION

In the mining and aggregates industry, crushing operations are critical and costly processes within the mechanical crushing chain. Jaw crushers, widely used in primary and secondary crushing stages [1], as well as in mineral selection methods, such as magnetic separation, constantly face operational challenges that have significant economic impacts on extractive operations, as machinery components and devices are subject to wear and corrosion during operation. Although jaw crushers can achieve high production compared to other crushers, they have high wear rates. Therefore, they must maintain a balance between efficiency and durability, making it essential to understand the mechanisms that govern the wear of critical components, which significantly determine the reliability indices for mining productivity [2, 3].

The wear in crusher components mainly results from a combination of abrasion, impact, and plastic deformation. The resistance to wear depends strongly on the microstructural response of the material under cyclic loading and strain hardening, particularly in Hadfield steels [4, 5]. Several studies have analysed how compression and sliding conditions influence wear behaviour

and energy consumption in crushing equipment [6]. The works of Chen et al. [7] and Zambrano et al. [8] also provide insights into impact wear mechanisms and plastic deformation under severe service conditions.

The components of this equipment, particularly the jaws, are subjected to extreme working conditions, severe abrasion, and permanent contact with highly erosive materials. The progressive wear of the linings constitutes the main source of problems, as it gradually modifies the original geometry of the equipment, directly affecting its performance and operational efficiency [9, 10]. Ferritic manganese alloys (also known as Hadfield alloys in recognition of their creator) are widely used in the equipment exposed to wear and impact-abrasion conditions, such as mineral material fragmentation, grinding equipment coatings, and railway crossings [11, 12]. Hadfield steels are widely used in the equipment subjected to abrasive wear and impact due to their superior work hardening. Their mechanical behaviour is related to martensitic transformations, dislocation interactions and twinning, mechanisms dependent on the stacking fault energy characteristic of austenite [4, 5].

In mining and construction, impact wear is a distinctive form of material deterioration that is frequently observed [13], characterised by the interaction between collision and abrasive sliding processes. This mechanism predominates on surfaces that are in direct contact with fragmented material. The abrasive phenomenon is highly persistent over time, and the results obtained in wear tests are significantly affected by the mechanical and abrasive characteristics of the rock used during the experiment [14]. Abrasive wear causes microstructural alterations, manifested as plastic deformations and microcracks in the surface roughness located in the contact coatings subjected to friction [7].

The wear in jaw crushers is a complex process caused by the interaction of mineral particles with the jaw surfaces under severe operating conditions. The dominant mechanisms include abrasive wear, produced by the sliding and rolling of hard particles that progressively remove material and alter the jaw geometry; impact wear, generated by the repeated collisions of large fragments that induce plastic deformation, surface fatigue, and crack initiation [13]; adhesive wear, which occurs when particles adhere to and detach from the jaw surface, removing small fragments of the liner; and fatigue wear, resulting from cyclic stresses during continuous crushing that propagate microcracks and weaken the material. Among these mechanisms, abrasive and impact wear are the most significant in mining applications, as they directly reduce the service life of the jaws and compromise crushing efficiency.

Experimental wear tests by abrasion or erosion are usually carried out using laboratory-scale jaw crusher-type equipment, the constructive and economic limitations of which prevent the versatile modification of the particles and the morphological configuration of the surfaces subjected to wear [14]. Likewise, the erosive characteristics and the inherent physical properties of the material to be crushed are the variables that have a significant influence on the results obtained in experimental abrasion analyses. Several investigations addressed the wear in jaw crushers [6, 13].

The advancements in computational methods have made the discrete element method (DEM) a fundamental tool for simulating particle fragmentation in mining machinery, successfully expanding into agriculture, mining, and engineering. The versatility of the DEM approach lies in its ability to model granular systems by representing individual particles and their interactions. To represent particle breakage, the simulation uses the particle replacement model (PRM) that is integrated into EDEM and other software, a model that is a modification of the Hertz Mindlin contact model [1, 15]. In crushing, Quist and Evertsson developed a study of the Svedala H6000 cone crusher, combining experimental measurements with DEM simulations [14]. In turn, Jiang et al. implemented a hybrid methodology that integrates DEM with the Archard wear model to analyse crusher linings [8, 16]. The application of the DEM method has also been extended to high-pressure grinding equipment [16]. Recent computational advances have allowed the use of DEM to investigate the crushing behaviour and wear in different types of crushers. For instance, Jiang et al. [8] applied a bonded particle model in DEM to study iron ore fragmentation in cone crushers, demonstrating how operational parameters, such as eccentric speed and closed side setting directly influence throughput, energy consumption, and liner wear.

Advances in fracture modelling within the DEM framework have been particularly notable, with the contribution of Tavares standing out, who proposed an efficient fracture model based on spherical representations. This approach has been successfully implemented in commercial

platforms such as EDEM, facilitating its adoption in industrial applications [17]. In recent years, the Tavares breakage model was used in various crushers such as mills. Barrios and Tavares employed an integrated simulation methodology combining multi-body dynamics (MBD) and DEM [18,19]. Rodríguez et al. implemented the DEM-MBD-PRM computational simulations to thoroughly investigate the wear conditions on the operational performance of the high pressure grinding rolls [17]. Wu S. and his team applied the DEM-MBD integration to evaluate the damping parameters on the vibrational behaviour of a gyratory crusher [11]. DEM alone is insufficient to characterise complex dynamic behaviours. Behaviours such as in jaw crushers, where eccentric displacement generates elliptical trajectories that are difficult to model on platforms such as EDEM. However, it is also necessary to identify the interaction parameters that form the basis for correctly simulating rock crushing. Therefore, material calibration represents an optimal methodological strategy for validating the particle-particle and particle-geometric surface interaction parameters, allowing the real behaviour of rocks and crusher grinding wheels to be simulated using the Hertz Mindlin [1], Archard wear and Tavares contact models.

Previous studies on crusher wear have employed both experimental and computational methodologies. Experimental investigations performed with laboratory-scale jaw crushers have provided valuable insights into abrasion and erosion mechanisms, but they are limited in scalability and versatility. Some works have demonstrated the effectiveness of austenitic manganese steels in resisting abrasion under impact conditions, while others have highlighted the influence of compression and sliding on energy consumption and wear. On the computational side, DEM has been applied to cone crushers, showing the potential of numerical approaches for capturing particle breakage. More recently, bonded particle models have been used to investigate ore fragmentation in cone crushers, linking operational parameters to throughput, energy, and liner wear. These contributions underline the complementary roles of experimental validation and advanced simulations in understanding crusher wear. This research focused on a comprehensive analysis of the size of rock fragments entering the crushing system, the geometric configuration of the crushing jaws, and the operational kinematics of compression crushing equipment. The current study comprises a comprehensive evaluation that examines abrasive wear as a function of the particle size of the processed particles and their dynamic interaction with the jaw profiles under actual industrial operating conditions. To address the limitations identified in previous approaches and improve predictive accuracy in crushing equipment simulation, this paper proposed a DEM-MBD-PRM simulation methodology in conjunction with the Tavares breakage model and the Archard wear model.

There is a significant gap in specific knowledge about the effect of abrasive particle size on material wear as well as abrasive and erosive behaviour in crusher jaws.

Most of these studies have been centred on cone and gyratory crushers, with limited attention to jaw crushers, particularly regarding the combined influence of feed particle size and jaw geometry on wear evolution. This represents a critical gap, since abrasive and impact wear in jaw crushers are strongly dependent on both the size distribution of feed material and the dynamic interaction with the jaw profiles. The novelty of the present work lies in coupling DEM, MBD, and PRM, together with the Tavares and Archard wear models, to provide a detailed assessment of how particle size and jaw geometry jointly affect abrasive wear and operational efficiency under realistic industrial conditions.

RESEARCH METHODOLOGY

Case study parameters

The material simulated in this research corresponds to copper ore, represented by particles of varying sizes. The particle sizes are considered for secondary crushing. Figure 1 depicts a typical copper sulphide ore processing plant, showcasing equipment, such as jaw crushers, impact crushers, a ball mill, a spiral classifier, and flotation machines used for concentrating copper minerals.

Table 1 shows the copper size distributions. Scenario 1 incorporates particles smaller than 50% of the maximum feed size; scenario 2 comprises particles larger than 50% of the maximum feed diameter. The third scenario combines the particles from scenario 2 (25%) with a predominant fraction from scenario 1 (75%). This approach allows for a comprehensive analysis of the effect of particle size on crushing performance, optimising

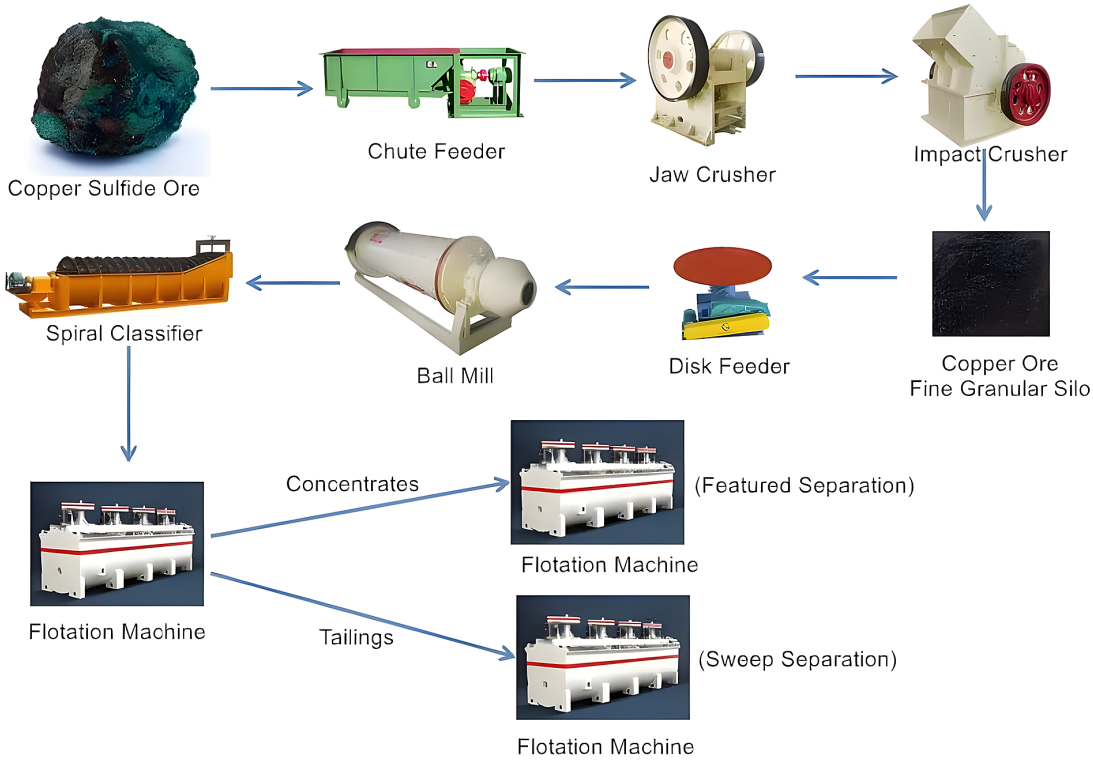

Figure 1. Copper sulphide ore processing flowsheet [20]

Table 1. Copper particle size distribution using DEM simulations

Sample	Particle size (mm)	Material	Particle size distribution %
1	[80–100]	Copper	100
2	[100–120]	Copper	100
3	[80–100]	Copper	75
	[100–120]	Copper	25

processing parameters and predicting mineral behaviour during comminution in copper mining.

The precise determination of the feed opening dimensions is a fundamental aspect in the design and efficient operation of crushing equipment. When selecting jaw crushers, various parameters must be evaluated, including the maximum dimensions of the materials that will enter the equipment and the required production capacity. The width and length of the feed opening were considered. References [21] and [22] are crucial as they provide the conceptual framework and the mathematical modifications required to derive Equations 1 through 7. Specifically, these references detail the decomposition of the W (Normal Load) and L (Sliding Distance) terms into variable components dependent on the motion of the movable jaw and the particle-liner interaction, enabling a detailed formulation of the local wear rate of the equipment. Equation 1 is used to determine the maximum diameter of particles entering (Dmax) based on the feed opening width (A) as follows:

$$D_{\max} = 0.8 \times A \tag{1}$$

Equation 2 shows that the feed opening length (L) is directly proportional to the width of the feed opening which is multiplied by a factor ranging from 1.5 to 2. These factors are correlated the length and width as follows:

$$L = (1.5 \ldots 2) \times A \tag{2}$$

Both dimensions of the crusher feed opening are shown in Figure 2. On the basis of the maximum size of the rocks, it was decided that the jaw crusher model should be an APJ-2540E 250 × 400. Figure 3 shows the design of the crusher, and Table 2 shows its parameters.

Material properties and parameters

Material properties are those that represent the material, such as modulus of elasticity (or shear modulus), solid density, and Poisson's ratio. Table 3 presents the individual properties of the material and austenitic steel, which were selected based on the research of Moncada et al. [11,

Figure 2. Feed opening dimensions in mm

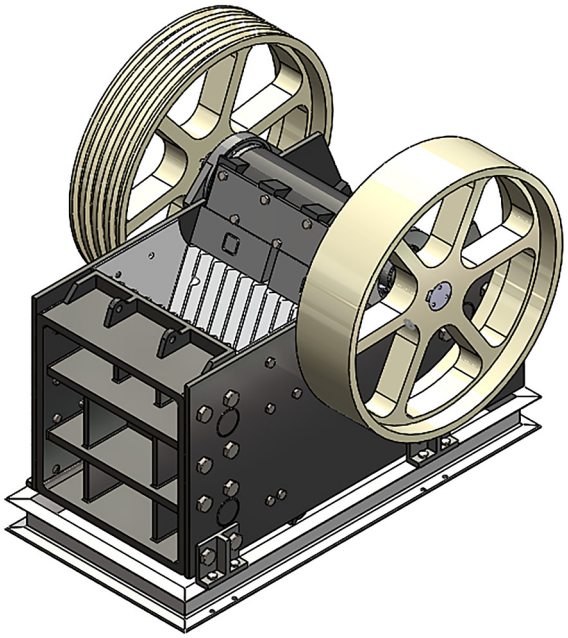

Figure 3. The crusher model used in simulation

24]. Contact parameters define the contact forces that calculated by the contact models and these parameters responsible for particle movement. The values of these parameters depend on the two materials in contact. These values were carefully selected considering the physical characteristics of the copper ore and the properties of the austenitic steel used in the construction of the crushing equipment. Table 4 shows the interaction properties, which were established based on the research by Moncada et al. [24]. The coefficients of friction, restitution, and adhesion were calibrated by comparing them with the experimental data from the article by Moncada et al. The material and contact properties in Tables 3 and 4 were used both in the calibration of the parameters and in the DEM simulations of the jaw crusher. This dual methodology made it possible to verify the

Table 2. Jaw crusher parameters [23]

Features	Value
Feed opening (mm)	250 × 400
Maximum feed size (mm)	210
Output size (mm)	20-80
Capacity (t/h)	5-20
Power (kW)	15
Overall dimensions (mm)	1450 × 1315 × 1296
Weight (t)	2.8

Table 3. Material properties in DEM simulations

Properties	Copper	Manganese steel
Density [kg/m^3]	2930	7850
Poisson's ratio	0.3	0.25
Young's modulus	1900 [Mpa]	190 [GPa]

Table 4. Properties of particles and steel

Parameter	Value
Restitution coefficient (PP) [1]	0.3
Restitution coefficient (PJ) [1]	0.3
Static friction coefficient (PP) [1]	0.25
Static friction coefficient (PJ) [1]	0.5
Rolling coefficient (PP) [1]	0.4
Rolling coefficient (PJ) [1]	4

Note: [1]PP : particle-particle; PJ: particle-jaw.

consistency of the model and optimise the input values to achieve greater accuracy in predicting the behaviour of the system. Figure 4 shows the two profiles of the two jaw models; model 1 has a sharp profile, and model 2 has a standard profile.

Discrete element method

The discrete element method (DEM) is a numerical simulation technique that solves the problems involving discontinuous media [26] by modelling the medium as discrete particles with specific properties and independent movement. Table 5 shows the considerations to be taken into account when simulating the difference between particles and geometry.

EDEM integrates base models, Hertz Midlin and Hertz Midlin with Johnson-Kendall-Roberts, the former for non-cohesive particles and the latter for cohesive particles. There are also contact models, [27, 28]. For the simulation, the base model used is the Hertz Midlin base model [21], the normal force is calculated using Equation 3 as follows:

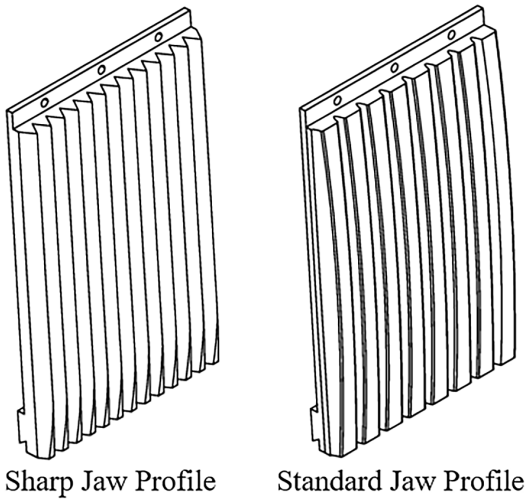

Figure 4. Jaw with a sharp profile and a standard profile [25]

Table 5. Comparison of particles and geometry

Particles	Geometry
Moving freely	Not moving freely
Affected by gravity	Not affected by gravity
Movement determined by collisions	Determining by movements created
Possible wear	Wear out
Created in EDEM	Created in another programme
Without mesh	Having mesh

$$F_n = \frac{4}{3} E^* \sqrt{R^*} \delta_n^{3/2} \tag{3}$$

where: Fn – normal contact force, E – reduced modulus of elasticity, R * – particle radius, normal overlap.

Equation 4 shows the modulus of elasticity of elements i and j as follows:

$$1/E^* = \frac{\left(1-v_i^2\right)}{E_i} + \frac{\left(1-v_j^2\right)}{E_j} \tag{4}$$

where: Ei – modulus of elasticity of element i, Ej – modulus of elasticity of element j, v_i – Poisson's ratio of element i, v_j – Poisson's ratio of element j.

Equation 5 shows the particle radius of elements i and j as follows:

$$1/R^* = \frac{1}{R_i} + \frac{1}{R_j} \tag{5}$$

where: R_i – particle radius of element i, R_j – particle radius of element j.

Equation 6 shows that the tangential force is calculated as follows:

$$F_t = S_t \delta_t \tag{6}$$

Equation 7 shows that the tangential stiffness is calculated as follows:

$$S_t = 8G^* \sqrt{R^* \times \delta_n} \tag{7}$$

where: Ft – tangential force, St – tangential stiffness, δt – tangential overlap/displacement, $G*$ – shear module.

Tavares' breakage model

Tavares' Universidade Federal do Rio de Janeiro model captures the fracture mechanisms in particle collisions, determining the final particle size distribution and establishing fragmentation processes for brittle materials. It considers dimensional variability, probability of rupture, and deterioration due to cyclic loads. In comminution, particles suffer impacts that are insufficient for immediate fracture, but their repetition accumulates the energy that generates internal deterioration similar to microcracks, progressively weakening them. This increases their vulnerability, allowing subsequent impacts with less energy to cause rupture. This process is called particle damage accumulation [29, 30]. EDEM detects these impacts, calculates the absorbed energy, and updates the residual fracture energy according to the accumulated damage [31].

Particle replacement model

A parent particle is replaced by several daughter particles, each time the first particle is subjected to a force that exceeds the maximum permitted value [32]. The fragmentation intensity is quantified by the single parameter t_{10}, which indicates the fraction of fragments the size of which is less than one-tenth of the initial particle dimension [33]. Figure 5 shows the particle replacement method, developed with the Universities of Rio de Janeiro and Edinburgh. Table 6 shows the copper breakage parameters that were established based on the research of Moncada et al. [24], who conducted a study on the crushing of copper with a cone crusher.

Archard wear model

The Archard Wear model extends base models for estimating wear depth, based on the principle

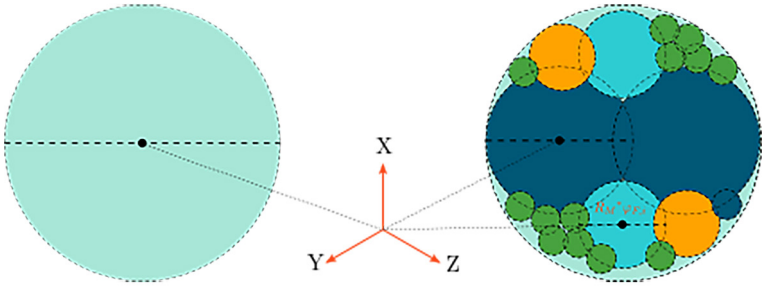

Figure 5. Particle replacement [19]

Table 6. Breakage parameters for copper

Parameter	Unit	Value
E50 parameter (d_0)	[mm]	8.07
E50 parameter (E_∞)	[J/kg]	213.5
Adjustment parameter (ϕ)	[-]	1.22
Standard deviation of fracture energy (σE)	[-]	0.799
Constant damage (γ)	[-]	0.3
Alpha percentage (α)	[%]	67.7
Impact fracture parameter used in the calculation of t_{10}, (b')	[-]	0.029
Minimum particle size for fracture (d_{min})	[mm]	5–100
Minimum collision energy (E_{min})	(J)	1
Shear energy fraction (C_t)	[-]	1

Note: E_{50} (d_0) – characteristic size parameter, $E\infty$ – fracture energy at infinite size, ϕ – fitting parameter, σE – standard deviation of fracture energy, γ – damage constant, α – percentage of broken particles, b' – impact fracture parameter used for t10, d_{min} – minimum particle size for fracture, E_{min} – minimum collision energy, and Ct – shear energy fraction.

that material removal is proportional to the frictional work exerted by moving particles [15, 27]. Equation 8 shows the mathematical model of Archard's equation.

$$\Delta V = w \times F \times d_t \tag{8}$$

where: ΔV – removed material volume, w – wear constant, d – tangential distance travelled, F – tangential force.

Equation 9 shows that the variation in volume is related to the variation in shear work and the wear constant [22].

$$\Delta V = \frac{k}{H} \times \Delta Wc \tag{9}$$

where: k – dimensionless constant characteristic of the material, H – Vickers hardness of the softest surface (in Pa), ΔWc – shear work variation.

For its implementation, it is simplified to a single wear constant to facilitate its integration into the EDEM software; this simplification maintains the physical essence of the phenomenon. In other words, the same actual volume loss can be achieved if the constant is increased. The same wear will be presented in less time for the simulation in comparison of what would happen in reality. Equation 10 shows the accelerated constant () that can be calculated based on the acceleration factor (a) and constant characteristic of the material (k) as follows: [34]:

$$C_{accelerated} = a \times k \tag{10}$$

Equation 11 is used for predicting the material volume to be removed as follows [35]:

$$\Delta V = a \times \frac{k}{H} \times \Delta Wc^* \tag{11}$$

The input to EDEM corresponds to the wear constant with units 1/Pa, allowing direct calibration with the experimental data. Figure 6 shows the methodology used in a flow chart, identifying the cycle experienced by the particle during impact.

Material calibration

This procedure seeks to accurately replicate the mechanical behaviour of granular material, ensuring that virtual simulations accurately reflect the wear and fragmentation characteristics observed under real mining conditions. Figure 7 shows the geometry used to represent the rocks for material calibration.

It is also recommended that following a normal distribution with respect to size be much more realistic than a fixed distribution. Figure 8 shows the distribution of particles, using the normal distribution. Figure 9 shows that the calibration method in EDEM follows a systematic approach that begins with understanding and classifying the

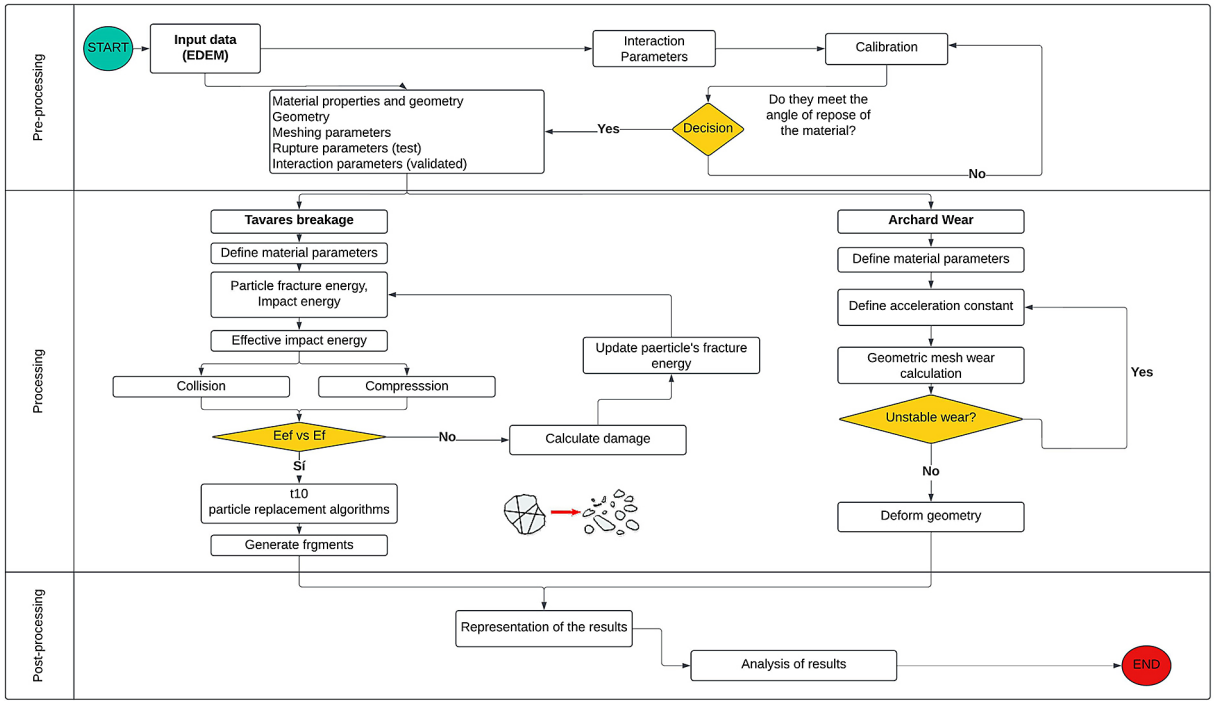

Figure 6. Flow chart of simulation pre-processing, processing, and post-processing

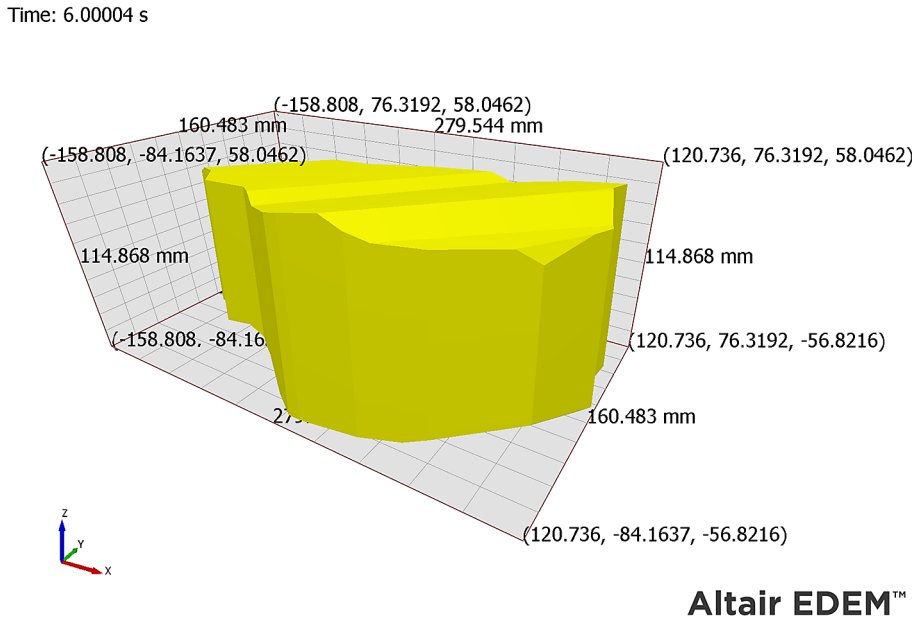

Figure 7. Particle representing copper rock

material to be modelled, followed by understanding the physical process to be simulated. Subsequently, the experimental test is reproduced within the virtual environment of EDEM, maintaining the same boundary conditions and geometry as the actual experiment. Figure 10 shows the calibration with particles, the geometry of which is similar to that of a rock, as shown in Figure 7. This granular material, modelled in the Altair EDEM software, is allowed to fall freely onto a surface, forming a cone and validating the behaviour of the particles. After the calibration simulation, the angle obtained from the script validates the angle of repose after several simulations until the appropriate parameters are found. Figure 11 shows the measurement of the angle of repose of the rocks or particles.

The spatial distribution of the particles shows the initial configuration of the material at rest,

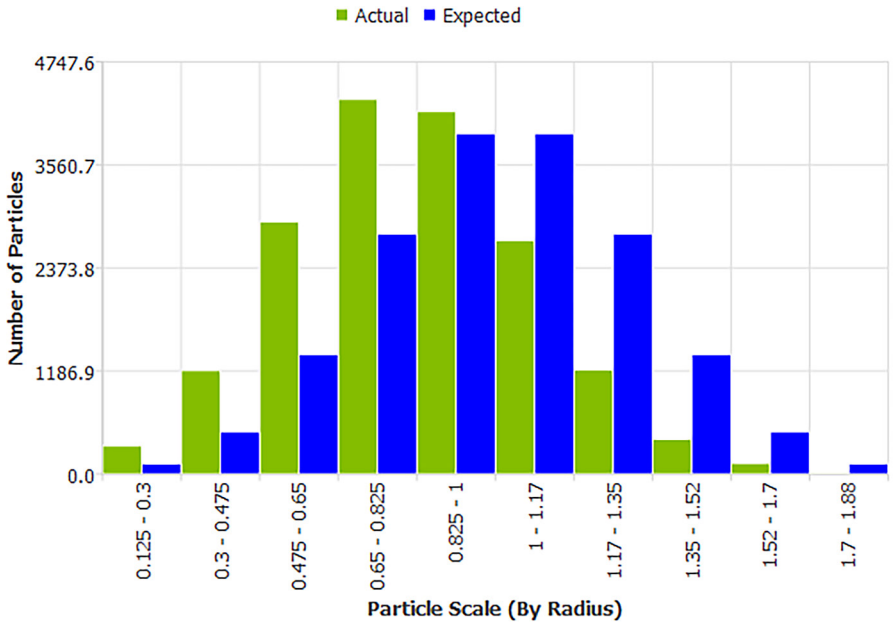

Figure 8. Particles number distribution for calibration

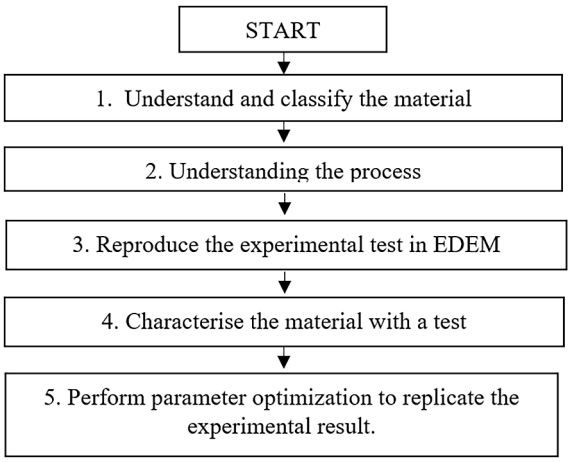

Figure 9. EDEM software methodology for calibration

where each granular element maintains its individual properties of shape, size and density, establishing the boundary conditions necessary to evaluate the behaviour of the whole during interaction with the jaw crusher using DEM simulation.

RESULTS AND DISCUSSION

Figure 12 shows a snapshot of the DEM simulation of crushed particles in the virtual jaw crusher. From a symmetrical cutting plane, particle breakage, modelled using the Tavares Model, can be observed. Figures 13 and 14 show the velocity and impact directions of the particles during crushing.

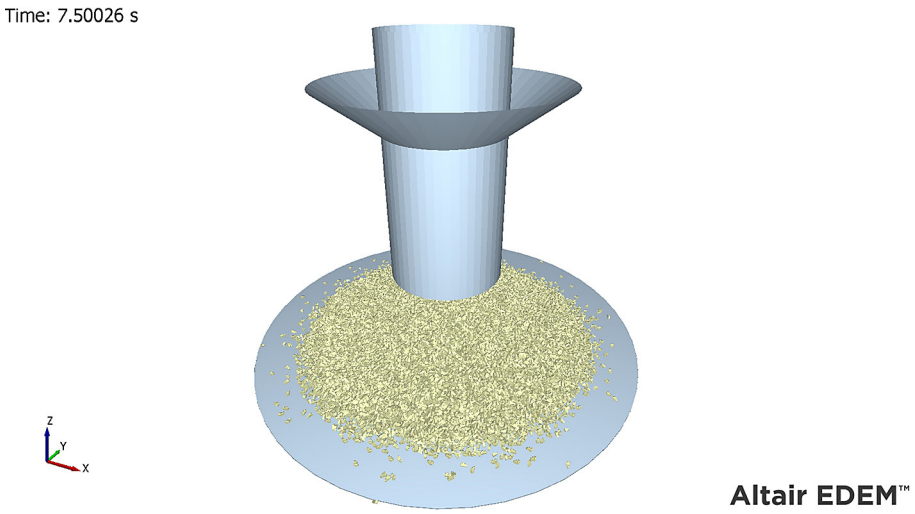

Figure 10. Final stage of material calibration

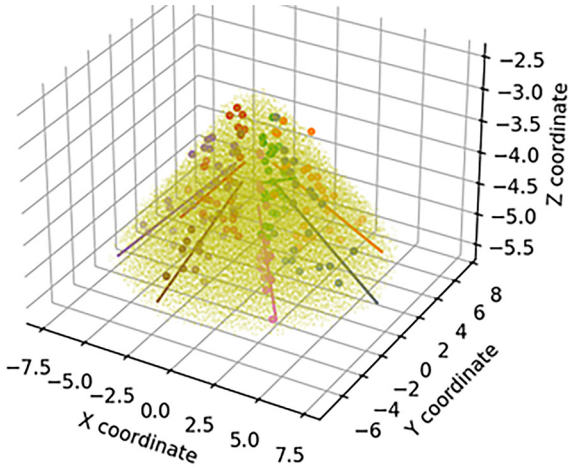

Figure 11. Particle calibration process

The acceleration constant or the sharp-edge jaw was $2 \times 10(^{-8})Pa^{-1}$ and for the standard profile jaw it was $2 \times 10(^{-9})Pa^{-1}$, because if the same value is taken for the standard profile jaw, it triggers unstable wear. In Figure 13, the highest velocities are near the discharge, due to the freedom of the rocks to exit as they become smaller. Similarly, in Figure 14, the impact directions are mostly present in the discharge zone. The results reflect that the DEM model effectively simulates the actual dynamics of crushers [36]. On the other hand, Figure 15 shows that the wear on the movable jaw has maximum values of 6.58e+01 mm in the areas of greatest contact with sample 2, which consists of large particles. This demonstrates that the particle size of the processed material significantly influences wear patterns, with greater intensity observed in the lower region of the jaw where the compressive forces are concentrated. The particles in sample 3 generate more uniform wear patterns on the jaw compared to the larger particle size samples.

Similarly, a more detailed comparison is shown in Figure 16 of the jaw model with a sharp profile, which shows that the wear on the fixed jaw has maximum values of 4.26e+01 mm in the areas of greatest contact with sample 2. The particles in sample 3 also generate more uniform wear patterns compared to the wear of the larger particle size sample, but sample 1 generates the least wear compared to the other two particle size samples of the material, suggesting a direct correlation between particle size distribution and component life.

On the other hand, an illustrative comparison is shown in Figures 17 of the movable jaw of jaw model 2 with a standard profile. This comparison shows that the wear on the movable jaw has maximum values of 4.19e+01 mm in the areas of greatest contact with sample 2. The behaviour is similar in the fixed jaw. The particles in sample 1 generate the wear patterns concentrated in the lower part, with a lower volume loss compared to the wear of the larger granulometric samples. Similarly, an illustrative comparison is shown in Figure 18 of the standard profile jaw model, which shows that wear on the fixed jaw has maximum values of 2.42e+01 mm in the areas of greatest

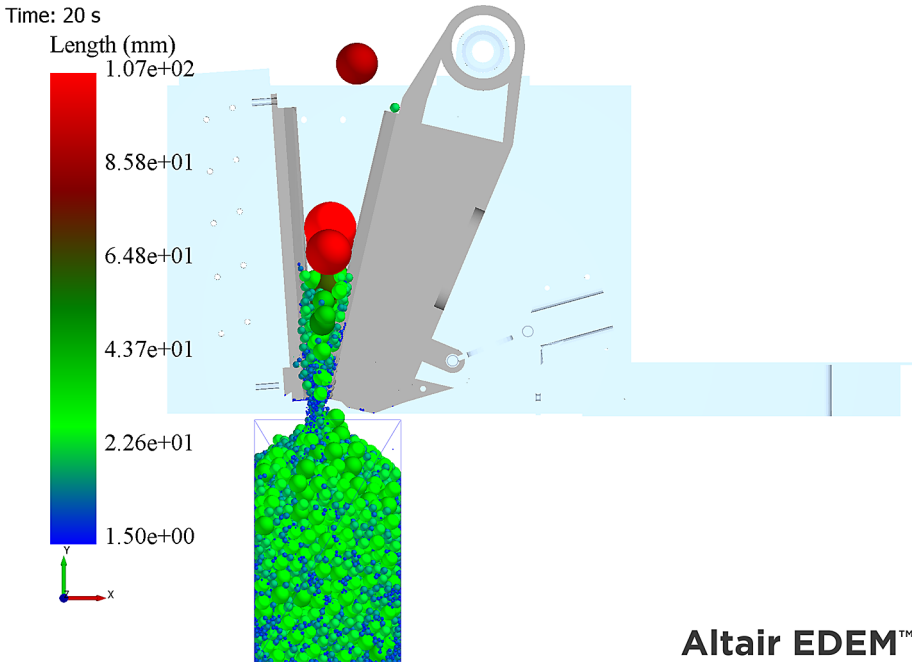

Figure 12. DEM simulation view of jaw crusher

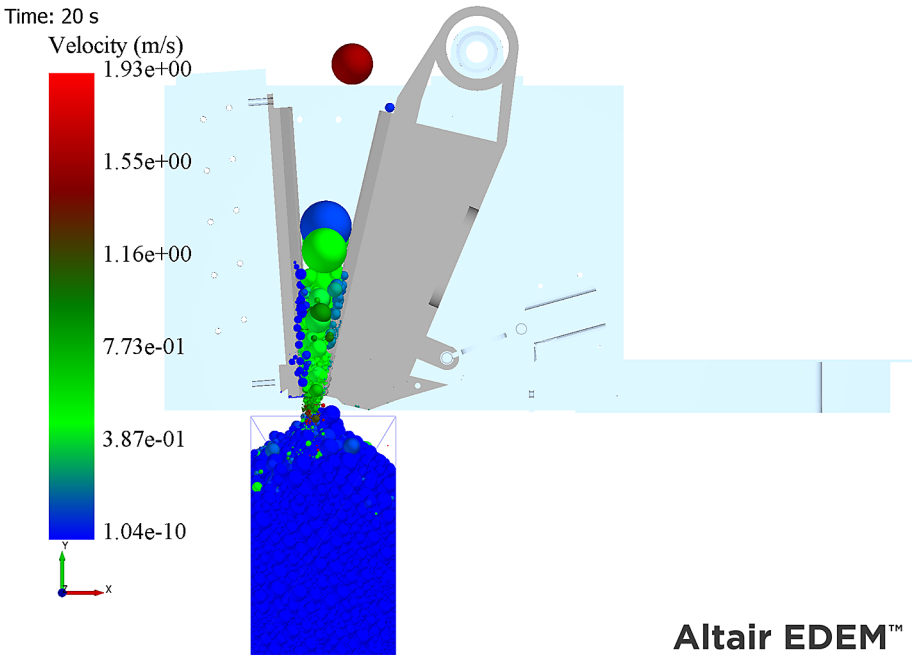

Figure 13. Particle velocity

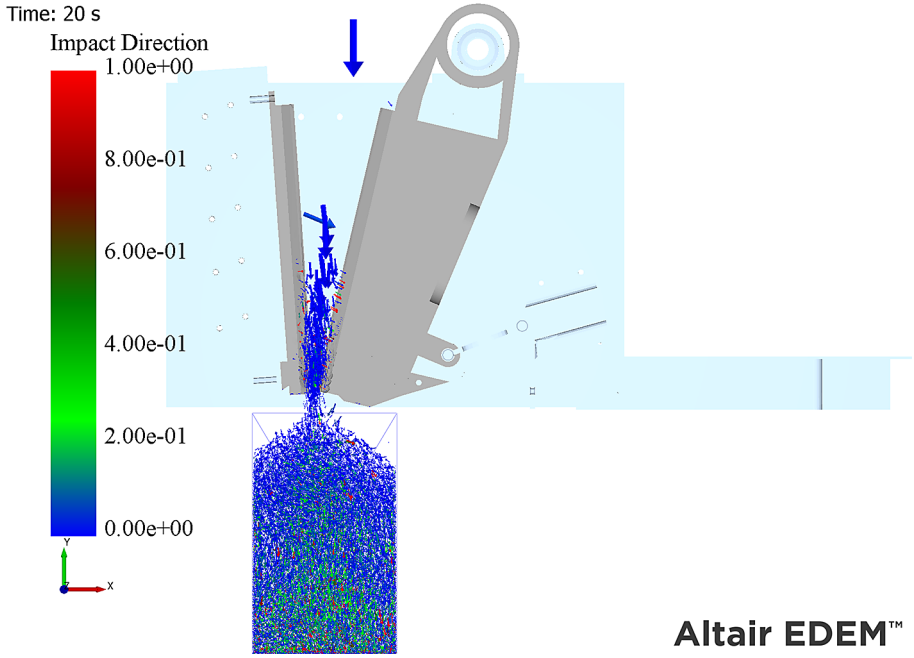

Figure 14. Particle impact direction

contact with sample 2. The particles in sample 3 also generate more uniform wear patterns compared to the wear of the larger grain size samples (sample 2), suggesting a direct correlation between grain size distribution and component life. However, the comparison in terms of wear time is shown in Figures 17a and 17b.

Figures 19 and 20 show the wear of the movable and fixed jaws for each of the three copper grain size samples, over a period of 10 seconds for jaw model 1. Sample 2 shows the greatest wear on both the fixed and movable jaws. The wear behaviour according to the samples is the same for jaw 2, which shows that the increase in size and uniformity results in greater wear than smaller particles.

The wear of 1 inch in 700 hours is a reference for the three cases of wear, the value of which allowed comparing the time it takes to achieve 1 inch of wear for each of the three cases of rocks and jaws. The times it takes to achieve this wear

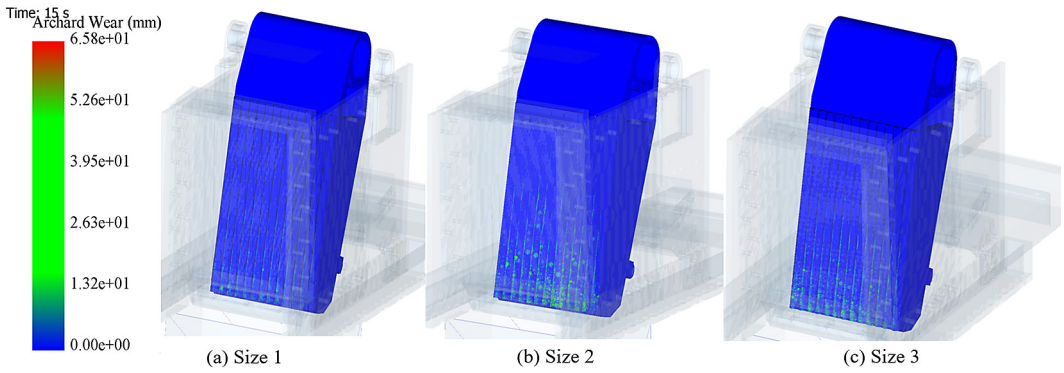

Figure 15. Wear of movable jaw 1 at: (a) sample size 1; (b) sample size 2; (c) sample size 3

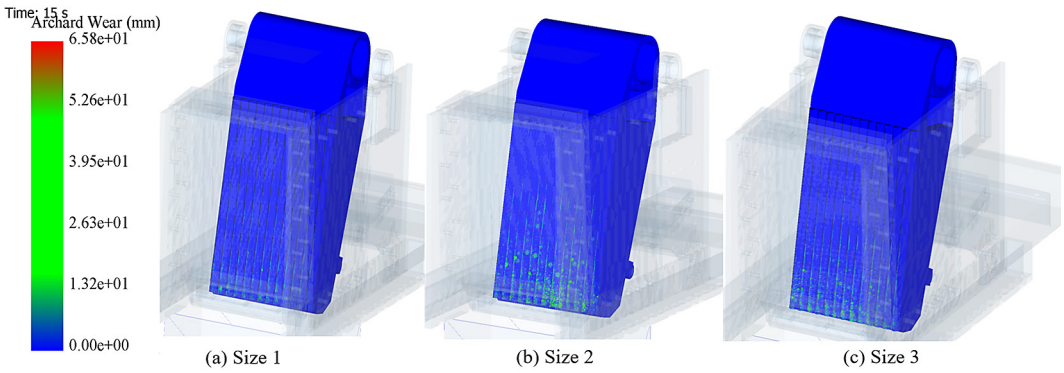

Figure 16. Wear of fixed jaw 1 at: (a) sample size 1; (b) sample size 2; (c) sample size 3

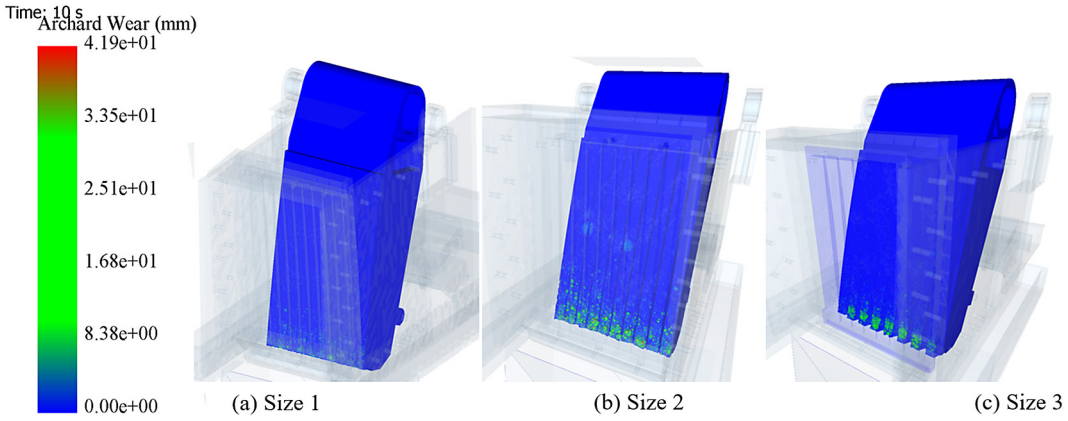

Figure 17. Wear of movable jaw 2 at: (a) sample size 1; (b) sample size 2; (c) sample size 3

are shown in Tables 7 and 8. In jaw 1, it was observed that the processing of smaller materials (Sample 1: 18s in simulation) resulted in a longer time for 1" wear to be achieved, exactly 787.5 hours for the movable jaw and 1584.90 hours for the fixed jaw. In contrast, processing larger materials (Sample 2: 9s in simulation) showed a shorter time, recording 393.75 hours and 660.38 hours respectively, indicating that the jaw can wear out quickly if only large particles are fed into it. This trend suggests that larger materials generate greater mechanical stress and abrasion on the crushing components. The comparative analysis between the two jaws reveals different behaviours in terms of durability and wear resistance. The jaw with a sharp profile showed a different wear pattern, especially noticeable in sample 2, where the fixed jaw experienced a wear time of 600 hours compared to 660.38 hours for the standard jaw. Similarly, for sample 2, jaw 2 showed

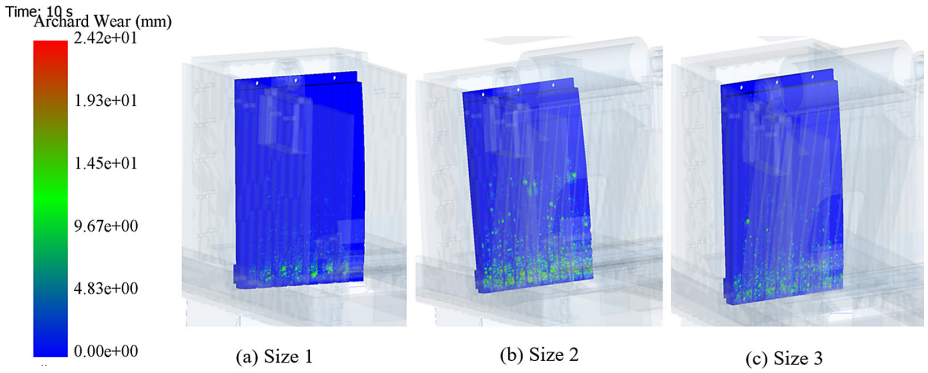

Figure 18. Wear of fixed jaw 2 at: (a) sample size 1; (b) sample size 2; (c) sample size 3

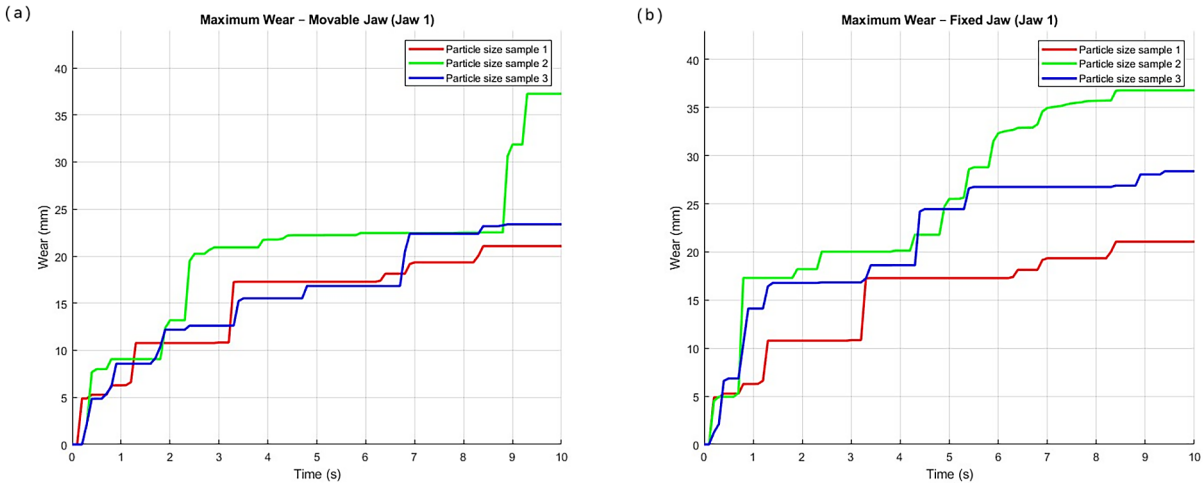

Figure 19. Comparison of wear at: (a) movable jaws of model 1, (b) fixed jaws of model 1

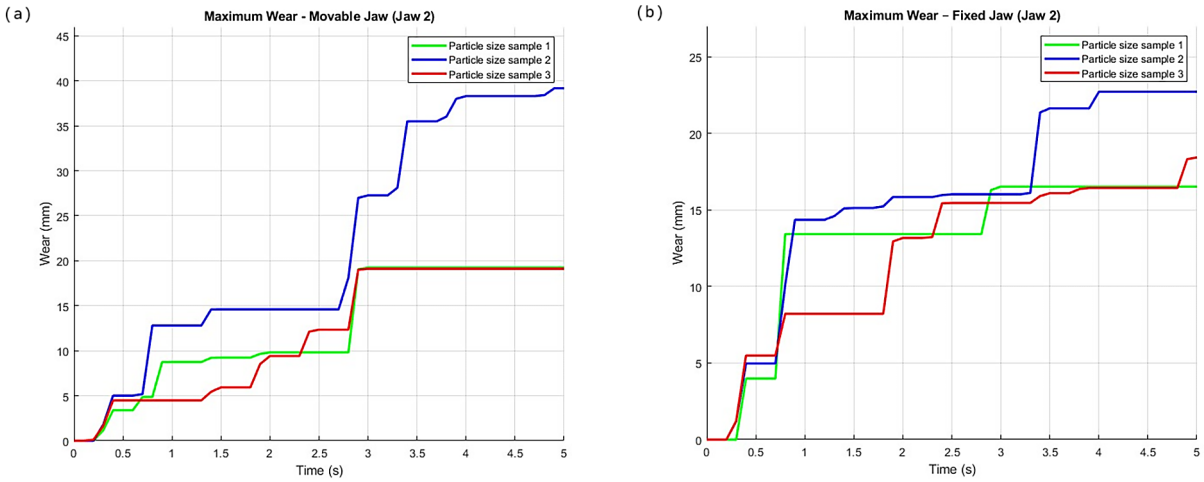

Figure 20. Comparison of wear at: (a) movable jaws of model 2, (b) fixed jaws of model 2

245 hours of wear on the moving part compared to 393.75 hours for jaw 1. These differences are attributed to variations in design. In terms of operational efficiency, the data indicate that feed size is a critical factor in optimizing the service life of crushing equipment. Jaw 1 demonstrated better overall performance in terms of wear resistance, particularly for smaller materials, making it an important factor in not accelerating wear time due to a uniformly larger size ranging from

Table 7. Equivalent wear on the jaw with a sharp profile

Sizes	Mobile jaw simulation	Hours (mobile jaw)	Fixed jaw simulation	Hours (fixed jaw)
Sample 1	18 [s]	787.5 [H]	9 [s]	1584.90 [H]
Sample 2	9 [s]	393.75 [H]	5 [s]	660.38 [H]
Sample 3	16 [s]	700 [H]	7 [s]	700 [H]

Table 8. Equivalent wear on the jaw with a standard profile

Sizes	Mobile jaw simulation	Hours (mobile jaw)	Fixed jaw simulation	Hours (fixed jaw)
Sample 1	9 [s]	787.5 [H]	11 [s]	1100 [H]
Sample 2	2.8 [s]	245 [H]	6 [s]	600 [H]
Sample 3	8 [s]	700 [H]	7 [s]	700 [H]

50 to 100% of the maximum diameter allowed in the operations requiring continuous processing.

CONCLUSIONS

This study addressed the critical problem of wear in jaw crushers, where abrasive and impact mechanisms strongly influence operational efficiency and equipment lifetime. Previous research has mainly focused on experimental abrasion tests or computational studies applied to cone and gyratory crushers, leaving a significant gap in understanding the combined influence of feed particle size and jaw geometry on wear behaviour in jaw crushers.

The novelty of this work lies in applying a coupled (discrete element method-multibody dynamics-particle replacement method) methodology, integrating the Tavares breakage model and the Archard wear model, to simulate industrial crushing conditions with calibrated material parameters. The results demonstrate that reducing feed particle size and optimising jaw geometry can decrease wear by up to 50%, directly improving crusher efficiency, reducing maintenance costs, and extending liner service life. These findings are consistent with previous reports on the dominant role of abrasive wear in crushing equipment, but they provide a more detailed quantification of how particle size distribution and jaw design interact to influence performance. The findings also have direct implications for both crusher manufacturers and mining operators. For manufacturers, the demonstrated influence of feed particle size and jaw geometry on wear provides valuable guidelines for designing more durable jaw profiles as well as selecting appropriate liner materials. For operators, the results indicate that controlling feed size distribution and optimising crusher settings can significantly extend liner lifetime, reduce maintenance frequency, and lower operational costs, while also improving energy efficiency.

Compared with earlier studies, this research advances the understanding of wear by explicitly linking particle-scale fragmentation with jaw kinematics and wear evolution. However, the study is limited by the simplifications inherent in numerical modelling, such as geometric assumptions and the calibration of contact parameters, which may affect direct extrapolation to all industrial contexts. Future work should focus on validating the proposed methodology with large-scale experimental tests, incorporating a wider range of rock types and liner materials, and extending the framework to analyse dynamic operating conditions, such as variable feed and energy consumption. These directions will enhance the predictive accuracy of wear modelling and contribute to the development of more durable and efficient jaw crusher designs.

Acknowledgments

This research has been carried out thanks to the support of the Universidad Nacional de San Agustín de Arequipa.

REFERENCES

1. Barrios GKP, Jiménez-Herrera N, Tavares LM. Simulation of particle bed breakage by slow compression and impact using a DEM particle replacement model. Advanced Powder Technology [Internet]. 2020; 31(7): 2749–58. Available from: https://www.sciencedirect.com/science/article/pii/S092188312030203X

2. Johansson M, Bengtsson M, Evertsson M, Hulthén E. A fundamental model of an industrial-scale jaw crusher. Miner Eng [Internet]. 2017 May 1 [cited 2025 Oct 31]; 105: 69–78. Available from: https://www.sciencedirect.com/science/article/pii/S0892687517300249?casa_token=_jjegLaINvkAAAAA:YLGp28x7yhcl0vWhvMew4juFED91rQg3-4uHT999pNb5-bhpR8sm8GDDANEp8ZlHVpApX4nZ8
3. Fladvad M, Onnela T. Influence of jaw crusher parameters on the quality of primary crushed aggregates. Miner Eng. 2020 Jun 1;151. https://www.sciencedirect.com/science/article/pii/S0892687520301588
4. Hai NH, Trung ND, Khanh PM, Dung NH, Long BD. Strain hardening of Hadfield high manganese steels. Mater Today Proc [Internet]. 2022; 66: 2933–7. Available from: https://www.sciencedirect.com/science/article/pii/S2214785322045904
5. Zambrano OA, Tressia G, Souza RM. Failure analysis of a crossing rail made of Hadfield steel after severe plastic deformation induced by wheel-rail interaction. Eng Fail Anal [Internet]. 2020; 115: 104621. Available from: https://www.sciencedirect.com/science/article/pii/S1350630720301448
6. Terva J, Kuokkala VT, Valtonen K, Siitonen P. Effects of compression and sliding on the wear and energy consumption in mineral crushing. Wear [Internet]. 2018; 398–399: 116–26. Available from: https://www.sciencedirect.com/science/article/pii/S0043164817313650
7. Chen X dong, Wang L wen, Yang L yun, Tang R, Yu Y qing, Cai Z bing. Investigation on the impact wear behavior of 2.25Cr–1Mo steel at elevated temperature. Wear [Internet]. 2021; 476: 203740. Available from: https://www.sciencedirect.com/science/article/pii/S0043164821001290
8. Jiang C, Gou D, Li C, Wu G, An X, Wang J, et al. Crushing characteristics and performance evaluation of iron ore in a cone crusher: A numerical study. Miner Eng [Internet]. 2023; 204: 108429. Available from: https://www.sciencedirect.com/science/article/pii/S0892687523004430
9. Sinha RS, Mukhopadhyay AK. Failure analysis of jaw crusher and its components using ANOVA. Journal of the Brazilian Society of Mechanical Sciences and Engineering [Internet]. 2016; 38(2): 665–78. Available from: https://doi.org/10.1007/s40430-015-0393-6
10. Maleki-Moghaddam M, Zare S. Investigating the chamber filling effect on the jaw crusher, cone crusher and HPGR performance. Canadian Metallurgical Quarterly [Internet]. 2025 Jul 3; 64(3): 1403–12. Available from: https://doi.org/10.1080/00084433.2024.2400727
11. Wu S, Wang S, Li X, Ye L, Shi P, Guo J, et al. Performance analysis of an experimental laboratory-scale eccentric roll crusher and a preliminary DEM-MBD coupled simulation method validation. Miner Eng [Internet]. 2025; 231: 109465. Available from: https://www.sciencedirect.com/science/article/pii/S0892687525002936
12. Khedr M, Li W, Min N, Elsheikh Ammar H, Jin X. Quantitative Evaluation of Deformation Mechanisms in Austenitic Hadfield Steel under Different Strain Rates. Steel Res Int [Internet]. 2025 Jul 1; 96(7): 2400714. Available from: https://doi.org/10.1002/srin.202400714
13. Machado PC, Pereira JI, Sinatora A. Abrasion wear of austenitic manganese steels via jaw crusher test. Wear [Internet]. 2021;476:203726. Available from: https://www.sciencedirect.com/science/article/pii/S0043164821001150
14. Quist J, Evertsson CM. Cone crusher modelling and simulation using DEM. Miner Eng [Internet]. 2016;85:92–105. Available from: https://www.sciencedirect.com/science/article/pii/S0892687515301230
15. Sun Y, Li Y, Zhang Q, Qin X, Chen K. Wear analysis and simulation of small module gear based on Archard model. Eng Fail Anal [Internet]. 2023 Feb 1 [cited 2025 Oct 31];144:106990. Available from: https://www.sciencedirect.com/science/article/pii/S1350630722009578?casa_token=NKBlGXsyn5gAAAAA:b7qOo2sDbhDtanNyo_jFwF_vbcQYF2dCnbmW9KnFS7BU3TSdEQ0zLNQGfgaOIXUjzBo7rVJ_YYY
16. Jiang H, Xu G, Zeng W, Gao F, Chong K. Lateral Stability of a Mobile Robot Utilizing an Active Adjustable Suspension. Applied Sciences [Internet]. 2019; 9(20). Available from: https://www.mdpi.com/2076-3417/9/20/4410
17. Rodriguez VA, Barrios GKP, Bueno G, Tavares LM. Investigation of Lateral Confinement, Roller Aspect Ratio and Wear Condition on HPGR Performance Using DEM-MBD-PRM Simulations. Minerals [Internet]. 2021; 11(8). Available from: https://www.mdpi.com/2075-163X/11/8/801
18. Tavares LM, das Chagas AS. A stochastic particle replacement strategy for simulating breakage in DEM. Powder Technol [Internet]. 2021; 377: 222–32. Available from: https://www.sciencedirect.com/science/article/pii/S0032591020308494
19. Ou T, Chen W. Modelling of Gyratory Crusher Liner Wear Using a Digital Wireless Sensor. Sensors (Basel). 2023 Oct 30; 23(21). https://www.mdpi.com/1424-8220/23/21/8818
20. JXSC Mineral. General Process of Copper Sulfide Ore Flotation [Internet]. 2024 [cited 2025 Oct 31]. Available from: https://www.jxscmineral.com/blogs/general-process-of-copper-sulfide-ore-flotation/
21. Horabik J, Beczek M, Mazur R, Parafiniuk P, Ryżak M, Molenda M. Determination of the restitution coefficient of seeds and coefficients of visco-elastic Hertz contact models for DEM simulations. Biosyst

Eng [Internet]. 2017 Sep 1 [cited 2025 Oct 31]; 161: 106–19. Available from: https://www.sciencedirect.com/science/article/pii/S1537511017303604?casa_token=nDp7dKeknb0AAAAA:W_IPTsDuQRHv5sFuZ-0yIks_Sng8lhiYLkz8qK0CarlNQWk5DE3vBnPc3nI7Ef5mstMxfZ-6SEE

22. Hanief M, Charoo MS. Archard's wear law revisited to measure accurate wear coefficient considering actual sliding velocity. Mater Today Proc [Internet]. 2021 Jan 1 [cited 2025 Nov 1]; 47: 5598–600. Available from: https://www.sciencedirect.com/science/article/pii/S221478532102530X?casa_token=A7qMp2l2RVgAAAAA:ZVOr5WwHmLNwjJ8qfOIUQ7WrxHxOz0x68CrT-0KNyDx1yEDtF3mjkSOxVJCJ6_KIYVAcPfdxCxY
23. Wills BA, Finch J. Wills' mineral processing technology: an introduction to the practical aspects of ore treatment and mineral recovery. Butterworth-heinemann; 2015. https://books.google.com.pe/books/about/Wills_Mineral_Processing_Technology.html?id=uMWcBAAAQBAJ&redir_esc=y
24. Moncada M, Rojas C, Toledo P, Rodríguez CG, Betancourt F. Influence of Particle Shape and Size on Gyratory Crusher Simulations Using the Discrete Element Method. Minerals [Internet]. 2025; 15(3). Available from: https://www.mdpi.com/2075-163X/15/3/232
25. Dunne RC, Kawatra SK, Young CA. SME Mineral Processing and Extractive Metallurgy Handbook [Internet]. Society for Mining, Metallurgy & Exploration, Incorporated; 2019. (Sme Mineral Processing & Extractive Metallurgy Handbook). Available from: https://books.google.com.pe/books?id=4hKGDwAAQBAJ
26. Sameer M, Fred Higgs C. A novel approach for modeling wear at macro length and time scales in discrete element systems. Tribol Int [Internet]. 2026; 213: 110756. Available from: https://www.sciencedirect.com/science/article/pii/S0301679X25002518
27. Shen X, Cao L, Li R. Numerical simulation of sliding wear based on Archard model. In: 2010 International Conference on Mechanic Automation and Control Engineering. 2010; 325–9. https://www.researchgate.net/publication/261074183_Numerical_simulation_of_sliding_wear_based_on_Archard_model
28. Liu Y, Liskiewicz TW, Beake BD. Dynamic changes of mechanical properties induced by friction in the Archard wear model. Wear [Internet]. 2019 Jun 15 [cited 2025 Oct 31]; 428–429: 366–75. Available from: https://www.sciencedirect.com/science/article/pii/S0043164818316971?casa_token=o-E8GCBotFEAAAAA:D_X3PSW_R1VRUR-59om4ENo7UIqRssudQ1Uft-8gqjwhPOZ_NTxXWCNxQkfi0NxfwA5ZMjizbC0
29. Zheng X, Shen Y, Yu H, Zhu Z, Du X. Sensitivity analysis of simulation parameters to evaluate the coarse-grain DEM for liner wear prediction. Minerals. 2025 Mar 1; 15(3). https://www.mdpi.com/2075-163X/15/3/305
30. Liu R, Shi B, Shen Y, Li G. Prediction model for liner wear considering the motion characteristics of material. Math Probl Eng. 2018; 2018. https://www.researchgate.net/publication/328765535_Prediction_Model_for_Liner_Wear_Considering_the_Motion_Characteristics_of_Material
31. Ding X, Rath P, Giraldo-Londoño O, Buttlar WG, Ma T. Fracture modeling of rubber-modified binder based on Discrete Element Method. J Clean Prod [Internet]. 2022; 380: 135017. Available from: https://www.sciencedirect.com/science/article/pii/S0959652622045905
32. Romanovich AA, Annenko DM, Romanovich MA, Apukhtina I V. Enhancing wear resistance of working bodies of grinder through lining crushed material. IOP Conf Ser Mater Sci Eng [Internet]. 2018; 327(3): 032007. Available from: https://doi.org/10.1088/1757-899X/327/3/032007
33. Tosun A, Konak G. Development of a model estimating energy consumption values of primary and secondary crushers. Arabian Journal of Geosciences. 2015 Feb 1; 8(2): 1133–44. https://link.springer.com/article/10.1007/s12517-013-1260-3
34. Forsström D, Jonsén P. Calibration and validation of a large scale abrasive wear model by coupling DEM-FEM: Local failure prediction from abrasive wear of tipper bodies during unloading of granular material. Eng Fail Anal [Internet]. 2016 Aug 1 [cited 2025 Nov 1];66:274–83. Available from: https://www.sciencedirect.com/science/article/pii/S1350630716301431?casa_token=lKDEuMJxVbgAAAAA:suEHHOteo8ITnRcB9XTLzr4gR3vywr81LhQ3lX2-35XWWDcLvJnIR8hnncuSP9eJHps8K7JxBNc
35. Chandan P, Das AP, Choudhury SS, Annabattula RK. A DEM-driven machine learning framework for abrasive wear prediction. 2025 Sep 10; Available from: http://arxiv.org/abs/2509.08637
36. Thompson JA, Berry L, Southern S, Walls WK, Holmes MA, Brown SGR. The effect of mesh discretisation on damage and wear predictions using the Discrete Element Method. Appl Math Model [Internet]. 2022 May 1 [cited 2025 Nov 1];105:690–710. Available from: https://www.sciencedirect.com/science/article/pii/S0307904X2200021X?casa_token=HcimrbF-m3YAAAAA:8vLMWUNumytnKEmh3KyjIZ-FN-cAI5Za9AJ60TnO2IjyrX88o2jlu-V2haPgr53TrgS0-KLVN6o